J Biomol NMR (2014) 59:219–230
DOI 10.1007/s10858-014-9840-4

ARTICLE

Nucleotide-type chemical shift assignment of the encapsulated 40 kbp dsDNA in intact bacteriophage T7 by MAS solid-state NMR

Gili Abramov · Amir Goldbourt

Received: 23 February 2014 / Accepted: 20 May 2014 / Published online: 30 May 2014

Abstract The icosahedral bacteriophage T7 is a 50 MDa double-stranded DNA (dsDNA) virus that infects *Escherichia coli*. Although there is substantial information on the physical and morphological properties of T7, structural information, based mostly on Raman spectroscopy and cryo-electron microscopy, is limited. Here, we apply the magic-angle spinning (MAS) solid-state NMR (SSNMR) technique to study a uniformly ^{13}C and ^{15}N labeled wild-type T7 phage. We describe the details of the large-scale preparation and purification of an isotopically enriched phage sample under fully hydrated conditions, and show a complete ^{13}C and a near-complete ^{15}N nucleotide-type specific assignment of the sugar and base moieties in the 40 kbp dsDNA of T7 using two-dimensional ^{13}C–^{13}C and ^{15}N–^{13}C correlation experiments. The chemical shifts are interpreted as reporters of a B-form conformation of the encapsulated dsDNA. While MAS SSNMR was found to be extremely useful in determining the structures of proteins in native-like environments, its application to nucleic acids has lagged behind, leaving a missing ^{13}C and ^{15}N chemical shift database. This work therefore expands the ^{13}C and ^{15}N database of real B-form DNA systems, and opens routes to characterize more complex nucleic acid systems by SSNMR.

Keywords Magic angle spinning · Solid state NMR · T7 bacteriophage · dsDNA · Chemical shift assignment · Virus

G. Abramov · A. Goldbourt (✉)
School of Chemistry, Raymond and Beverly Sackler Faculty of Exact Sciences, Tel Aviv University,
69978 Ramat Aviv, Tel Aviv, Israel
e-mail: amirgo@post.tau.ac.il

Introduction

Bacteriophage T7 is a 50 MDa virus that infects rough F^- *Escherichia coli* strains. It is composed of a 40 kbp double-stranded DNA (dsDNA) molecule, which comprises over half of the total viral mass (26 MDa) with nearly equal distribution of the four nucleobases adenine (27.2 %), thymine (24.4 %), guanine (25.8 %) and cytosine (22.6 %). The dsDNA is wrapped around an internal cylindrical protein core (Cerritelli et al. 2003), and enclosed in an icosahedral capsid, which is made of hundreds of repeating protein subunits (Agirrezabala et al. 2005; Ionel et al. 2011). A ring-shaped complex, known as the connector, joins the internal core through one capsid vertex to an external short tail, which attaches six fiber proteins used during the process of infection (Cuervo et al. 2013). This complex viral assembly is one of the most studied among the dsDNA viruses both from a biochemical and a biophysical point of view. The mechanical properties and the morphology of T7 and various other packed viral genomes, have been studied mostly by cryo-electron microscopy (Cerritelli et al. 1997; Jiang et al. 2006; Duda et al. 2009), molecular dynamics simulations (Petrov et al. 2007), and single-molecule techniques (Ben-Shaul 2013). It was found that the genome packaging mechanism is highly conserved among many DNA viruses, including tailed dsDNA bacteriophages such as T7 (Black and Thomas 2012). It was shown that its large genome is packed into a preformed capsid (procapsid) within minutes by using an ATP-driven molecular motor (Daudén et al. 2013). Often, the packaged genome is bent because of its confinement within a capsid with comparable dimensions to its persistence length. Moreover, even though tailed phages have different interior capsid content, and capsid size and symmetry, their genomes are highly condensed to a comparable degree. Thus, in many ways the

genome of T7 can be used as a paradigm structure for natural, highly compacted and bent DNA in functional biological assemblies. In effect, tightly bent DNA is commonly found in nature, in viruses and in eukaryotic cells where it is organized in complex protein-DNA assemblies (nucleosomes).

Diverse models have been proposed to the conformation of the packaged DNA in different bacteriophages (Petrov et al. 2007). It was suggested that in T7, the DNA forms a set of rings around the protein core, and overall a coaxial spooling model best describes its conformation inside the capsid (Cerritelli et al. 1997). Most studies show that a tightly condensed and bent DNA is predominantly B-form (Deng et al. 1999). Raman studies of T7 phage report a B-form of its encapsidated dsDNA, characterized by a C2′-endo sugar pucker and an *anti* glycosyl orientation (Thomas and Serwer 1990; Overman et al. 1998). These studies also report that the packaged DNA has a phosphodiester geometry of an A-form DNA, specifically the C5′–O–P–O and O–P–O–C3′ torsion angles, designated α and ζ, respectively. However, this is a local geometry of the phosphodiester groups, and does not contradict the overall reported secondary structure of the packaged DNA. Moreover, the origin of this apparent deviation from a classic B-DNA phosphodiester geometry is probably due to the coiled nature of the wild-type genome.

The diversity and complexity of large biomolecules that can be structurally characterized has extended significantly with the introduction of magic-angle spinning (MAS) solid-state NMR (SSNMR) into this field of research. A considerable number of large biomolecular systems, which are non-crystalline, non-soluble, or have very high molecular weight, have been characterized by MAS SSNMR including membrane proteins (de Groot 2000; Cady et al. 2010; Park et al. 2012; Tang et al. 2013; Wang et al. 2013), fibrils forming proteins (Petkova et al. 2002, 2006; Jaroniec et al. 2004; Wasmer et al. 2008; Loquet et al. 2012; Lopez del Amo et al. 2012), and viruses (Goldbourt et al. 2007; Abramov et al. 2011; Han et al. 2013). Studies of these large systems, very much like solution NMR studies of proteins, rely partly on an extensive database of amino acid shifts, which are readily available in the Biological Magnetic Resonance Data Bank (BMRB)(Ulrich et al. 2008). Unlike this extensive database that can be readily associated with protein secondary and even tertiary structures (Wishart and Sykes 1994; Cornilescu et al. 1999; Berjanskii et al. 2006; Shen et al. 2009), nucleic acids studies by NMR, particularly in the solid state, are rather limited. These studies concentrated mostly on small DNA and RNA molecules, and on synthetic oligonucleotides (up to about one hundred nucleobases according to the BMRB).

The limited chemical shift database of nucleotide shifts, and in particular those of ^{13}C and ^{15}N, is a consequence of the small spectral dispersion and the small variety of four nucleic acid types. In addition, many nucleic acids base carbons (and nitrogens) are quaternary (tertiary), thus many proton-mediated NMR experiments (mostly in solution) provide limited structural information on these spin systems. Nonetheless, over the past years there has been substantial progress in establishing a chemical shift database of nucleic acids, particularly for RNA in solution (Wijmenga and van Buuren 1998; Fürtig et al. 2003; Barton et al. 2013). These studies focused on finding correlations between chemical shift values and structural information (Rossi and Harbison 2001; Ohlenschläger et al. 2008; Aeschbacher et al. 2013). Moreover, ^{13}C-direct detected NMR experiments were developed for the assignment of RNA oligonucleotides, which came from the realization that proton-deficient carbons in nucleic acids carry valuable conformational information (Fürtig et al. 2004; Fiala et al. 2004; Dayie 2005; Farès et al. 2007; Richter et al. 2010). The application of solution-state NMR to large DNA and RNA molecules is not straightforward since spectral resolution is highly dependent on molecular tumbling and therefore on molecular size. MAS NMR spectroscopy on the other hand has the potential to probe large and native systems since molecular weight does not affect line shape quality. In addition, the assignment of non-protonated species can benefit from the dipolar transfer mechanisms offered by a variety of SSNMR techniques.

Various recent reports have shown that experimental schemes routinely applied for SSNMR studies of proteins can be successfully adapted and optimized for structural studies of RNA and RNA–protein complexes (Riedel et al. 2004, 2005; Cherepanov et al. 2010). A notable example is the recent study of a 26mer box C/D RNA in complex with the L7Ae protein (Marchanka et al. 2013). In this study, a suite of two- and three-dimensional SSNMR experiments was developed and combined with nucleotide-selective labeling schemes to obtain intra-nucleotide resonance assignments. Other examples are the characterization of protein-RNA interfaces by ^{1}H-detected correlation experiments on protonated and deuterated samples (Asami et al. 2013) or by using ^{31}P heteronuclear correlations to observe contacts between the DNA or RNA and the protein moieties (Yu and Schaefer 2008; Jehle et al. 2010; Morag et al. 2014).

Although it was shown that SSNMR can provide detailed information on the conformation and environment of large DNA molecules (Sergeyev et al. 2011; Morag et al. 2014), a reliable chemical shift database is missing, which restrains the study of large natural DNA and RNA systems by NMR.

Here, we report our study of the B-form dsDNA of T7 phage using MAS SSNMR. We obtained a complete nucleotide-type specific ^{13}C and a near complete ^{15}N chemical shift assignment of the 40 kbp native genome by two sets of two-dimensional (2D) homo- and heteronuclear correlation experiments. Our results, which lay the basis for the study of large native DNA-containing systems by NMR, are compared to the chemical shift values reported for DNA and RNA oligonucleotides and to the prior assignment of ssDNA in fd filamentous virus (Morag et al. 2014).

Materials and methods

Preparation of T7 phage

The large-scale production of an isotopically labeled T7 phage was as follows; *E. coli* BW25113 cells were first grown in a nutritionally rich LB medium overnight. The culture was then diluted 1:200 into a minimal medium (21.1 mM Na_2HPO_4, 11.0 mM KH_2PO_4, 4.28 mM NaCl, 2 mM $MgSO_4{\cdot}7H_2O$, 0.1 mM $CaCl_2{\cdot}H_2O$, 18 μM $FeSO_4{\cdot}7H_2O$, and 1.48 μM thiamine-HCl), and supplemented with 5 g/L ^{13}C-glucose and 1 g/L $^{15}NH_4Cl$ (Cambridge Isotope Laboratories). It was then incubated at 37 °C with vigorous shaking (300 rpm) to a cell density of 10^8 bacteria/ml (corresponding to an optical density of 0.6 at 600 nm) and was then infected with a phage stock solution at a multiplicity of infection (moi) of 30. Cell lysis occurred 1–1.2 h from infection and the lysate was centrifuged to discard the cell debris. The phages in the supernatant were precipitated with 0.5 M NaCl and 10 % polyethylene glycol (PEG) 8000, and then purified by CsCl-gradient ultracentrifugation at 37,000 rpm for 48 h. The phage fraction, located at a buoyant density of 1.6 mg/ml was isolated and precipitated with 10 % PEG 8000 into a MAS NMR rotor. A standard plaque assay using the soft agar overlay technique (Sambrook et al. 1989) was performed in order to calculate the number of infectious phage particles, described in plaque-forming units (pfu)/ml. We obtain a yield of about 6×10^{12} phage particles per one liter of growth medium. A total of 10 l were used for the preparation of the NMR sample corresponding to a total mass of about 5 mg.

NMR spectroscopy

All MAS SSNMR spectra were acquired on a Bruker Avance III spectrometer operating at a 600 MHz ^1H frequency, and equipped with a 3.2 mm triple-resonance (^1H, ^{13}C, ^{15}N) Efree MAS probe. Carbon chemical shift assignments of the sugar and base atoms in T7 dsDNA were extracted from a two-dimensional (2D) homonuclear ^{13}C–^{13}C correlation experiment using the DARR/RAD sequence (dipolar-assisted rotational resonance/radio-frequency assisted diffusion) (Takegoshi et al. 2001; Morcombe et al. 2004) with a mixing period of 100 ms (DARR100). Nitrogen shifts of the nucleobases were assigned in a heteronuclear ^{15}N–^{13}C correlation experiment that was conducted using a ^{13}C-detect TEDOR (transferred-echo double resonance) sequence (Hing et al. 1992). In this version of TEDOR, ^{15}N transverse magnetization, obtained by cross-polarization (CP) from ^1H spins (Pines et al. 1973; Stejskal et al. 1977), was allowed to evolve during t_1. Then, the ^{13}C–^{15}N dipolar interaction was recoupled for a period of eight rotor cycles by the application of pairs of ^{15}N π pulses positioned at the middle and in the end of every rotor period (a single ^{15}N π pulse in the middle of this period was replaced by a ^{13}C π pulse thus generating a ^{15}N echo). Polarization transfer was obtained by the application of simultaneous ^{15}N and ^{13}C π/2 pulses, and was followed by a similar scheme lasting ten rotor periods. These time periods (8 and 10 rotor cycles corresponding to 533 and 667 μs) were found to be optimal for a transfer between directly bonded ^{13}C–^{15}N pairs, based on simulations using the SPINEVOLUTION program (Veshtort and Griffin 2006) and limited experimental optimizations. The acquisition parameters of both the DARR and TEDOR experiments are summarized in Table 1. For processing, all spectra were zero-filled to 16 k pts. in both dimensions. Both exponential and Lorentz-to-Gauss apodization functions with different broadening constants were applied in order to extract the required spectral

Table 1 Summary of the main MAS SSNMR acquisition parameters that were used in the 2D ^{13}C–^{13}C (DARR100) and ^{15}N–^{13}C (TEDOR) correlation experiments conducted on a uniformly [^{13}C, ^{15}N]-labeled T7 phage sample

	DARR100	TEDOR
Spinning rate	12 kHz	15 kHz
Temperature set	0 °C	−5 °C
Acquisition points (t_1/t_2)	800/4,990	256/4,990
Spectral width (t_1/t_2)	40/100 kHz	15/100 kHz
Carrier frequency	^{13}C 99.9 ppm	^{15}N 160 ppm ^{13}C 154 ppm
Radiofrequency field	^1H 85 kHz ^{13}C 50 kHz	^1H 100 kHz ^{15}N,^{13}C 50 kHz
CP contact time	1 ms	2 ms
^1H decoupling (SW_f-TPPM)[a]	85 kHz/6 μs	90 kHz/6 μs
Scans/recycle delay	128/3 s	440/3 s

t_1 and t_2 indicate the indirect and direct acquisition dimensions, respectively

[a] Thakur et al. (2006)

information, as detailed in the captions. Carbon chemical shift frequencies were referenced to the 40.48 ppm methylene line of adamantane (Morcombe and Zilm 2003) and nitrogen shifts were referenced to the signal from solid $^{15}NH_4Cl$ at 39.27 ppm (McDermott and Gu 1996). The data were processed using the NMRPipe software (Delaglio et al. 1995) and analyzed with the Sparky assignment program (Goddard and Kneller 2008).

Results and discussion

Optimal preparation and characterization of T7 phage

In order to prepare a suitable NMR sample of T7 phage, it was first necessary to find an optimized preparation protocol for obtaining pure isotopically labeled particles in sufficient amounts (approximately 5 mg). Thus, several growth conditions were tested and the final large-scale sample preparation protocol is detailed in the "Materials and methods" section.

The general bacteriological protocols are similar for different phage systems, and growth of a $^{13}C/^{15}N$ labeled T7 phage follows the principles underlying filamentous phages (Abramov et al. 2011). Yet, some adjustments are to be made for the specific phage, since T7 is expressed in a different *E. coli* strain and undergoes a different viral reproduction path. Being a lytic phage, the yield of T7 depends on bacterial concentration because at the end of the assembly process, the release of the phage particles from the cell involves its destruction. In the lysogenic cycle on the other hand (such as in fd filamentous phage), the cells remain intact after progeny release and are susceptible to more infecting phage particles. The general growth protocol of T7 in nutritionally rich medium, which was obtained from F.W. Studier (personal communication), is a slight modification of the original preparation protocol (Studier 1969). In this work, the procedure was modified and adapted for large-scale growth in minimal media. Overall, the yield of the uniformly ^{13}C and ^{15}N enriched T7 sample was ~1 mg per 2 l of minimal growth medium, which is similar to the reported yields in nutritionally rich media.

In order to obtain sufficiently pure particles, CsCl-gradient ultracentrifugation in a SW-41 swinging bucket rotor was performed for 48 h rather than a simple step gradient. We found that empty capsids of T7 particles are spontaneously formed, and band at a lower density than fully packed capsids. Therefore, those empty particles could also be isolated. The banding of different fractions in the Ultra-Clear™ 13.2 ml tube after centrifugation is shown in the inset of Fig. 1 as well as the electron microscopic image of the pure phages. The UV absorption spectra of T7

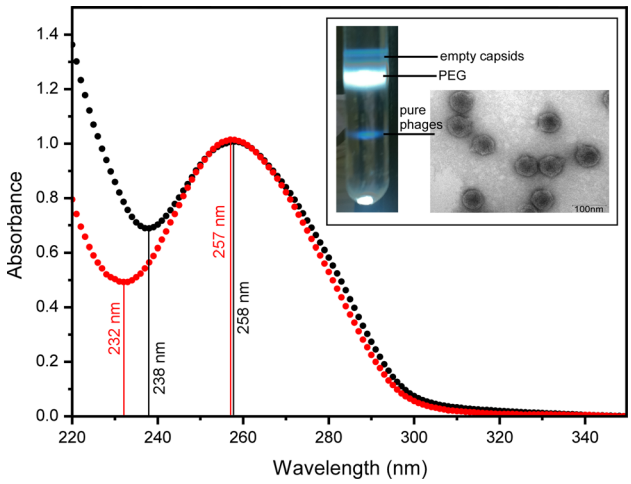

Fig. 1 UV absorption spectra of two T7 phage solutions prior (*black*) and after (*red*) density gradient ultracentrifugation. The *inset* shows a photo of the tube from the CsCl-gradient ultracentrifugation, where separated bands of the different fractions are indicated. The phage band at a CsCl density of 1.6 mg/ml was easily isolated, examined by UV (red spectrum) and imaged using electron microscopy (*inset*). The size and shape of the phage particles are consistent with previous reports (~60 nm) and show an intact virus. The spectrum of T7 resuspended in a TE buffer (10 mM Tris–HCl, pH 8.0, 1 mM EDTA) after the separation from the lysed cells (i.e. prior to ultracentrifugation) shows a minimum absorption at 238 nm and a maximum at 258 nm. The purified T7 particles show a similar maximum absorption, a larger ratio between the maximum and minimum values, and its minimum absorbance wavelength is blue-shifted to 232 nm

solutions, acquired on an 8453 UV–Vis Agilent spectrophotometer prior and after purification, are shown in Fig. 1. To the best of our knowledge, reports of such spectra are limited (Tóth et al. 1984). Generally, absorption in the near UV by a bacteriophage depends on the relative contents of the protein and polynucleic acid chain, DNA or RNA (Porterfield and Zlotnick 2010). Proteins usually show absorption maxima between 275 and 280 nm (with minimum at 250 nm), which are caused by the absorbance of the two aromatic amino acids tryptophan (Trp) and tyrosine (Tyr) and, to a small extent, by the absorbance of cysteine disulfide bonds (Goldfarb et al. 1951; Aitken and Learmonth 1996). DNA molecules have absorption minimum between 220 and 230 nm, and maximum between 253 nm (for guanosine) and 271 nm (for cytidine) that originates from π–π* transitions of the purine and pyrimidine rings (Schmid 2001). Therefore, they feature a broad peak at about 260 nm, which can be used for calculating their absorption coefficient (Henderson et al. 1992; Tataurov et al. 2008). The UV spectrum of T7 phage is consistent with typical spectra of pure DNA. This result is not surprising since the dsDNA in T7 constitutes the majority of the viral mass, and in addition, the extinction coefficients of nucleic acids are large compared to aromatic amino

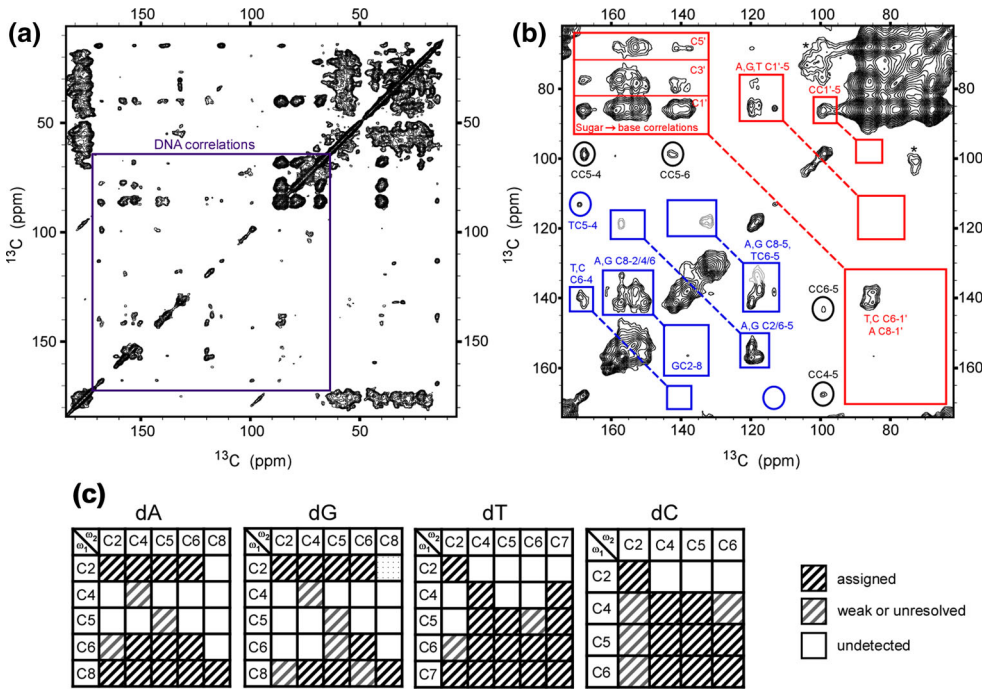

Fig. 2 2D ^{13}C–^{13}C DARR100 of the uniformly labeled T7 phage. **a** The full spectrum showing all carbon resonances originating from capsid (10–75, 170–185 ppm, aromatic residues at 120–160 ppm) and DNA (boxed region, dTC7 methyl signals at ~14.5 ppm and C2′ sugar signals at ~40 ppm) contributions. The acquisition parameters of the experiment are detailed in Table 1. The spectrum was processed with a Lorentz-to-Gauss transformation in both dimensions. **b** Extracted region from the same experiment (the boxed region from **a** processed with an exponential broadening of 200 Hz in both dimensions) showing the DNA region. Symmetrical regions across the diagonal are indicated and show a clear difference between protonated and unprotonated carbons. Some capsid resonances are *colored* in *grey*. **c** Schematic representation of the assigned cross-peaks, where each grid describes the resonance pathway of the different nucleobases; dA, dG, dT and dC. The *rows* represent spins excited by the CP process that appear in the indirect dimension and columns correspond to the directly detected spins after spin polarization was transferred from the excited spins. The correlations within each DNA base are symbolized according to the attained cross-peaks. For simplicity, deoxynucleotides in all figures are noted by the single letter codes A, G, C, T

acids, and may be as much as 10 times that of a protein. In fact, bacteriophages that are composed of over 80 % protein (such as the filamentous fd virus), have a maximum plateau at 265–270 nm, rather than at 280 nm (Day et al. 1988; Tomar et al. 2007). Moreover, there are no Trp residues in the T7 capsid and the Tyr residues constitute only about 3 % of the total capsid mass, thus, their contribution is small. The UV spectra overlay in Fig. 1, of a pure sample and a sample prior to ultracentrifugation, show that the minimum absorbance wavelength is shifted from 238 to 232 nm after purification, the maximum position is not changed (located at ~258 ppm), and the maximum to minimum ratio increases from 1.5 to 2.1 upon sample purification.

Nucleotide-type specific ^{13}C and ^{15}N assignment of the B-form dsDNA of T7

Assignment of DNA cross-peaks requires distinction between nucleotide-base signals and protein signals. The main similarity is observed for the aromatic signals of tyrosine, phenylalanine and histidine as well as the terminal part of the positively charged arginine residue. Yet, unlike fd, where blanking of these aromatic amino acids was essential for obtaining satisfactory DNA signals within the strong capsid signals (Morag et al. 2014), here we could easily differentiate between the capsid and dominant DNA resonances through their unique intra-nucleotide correlation patterns. The complete 2D ^{13}C–^{13}C correlation experiment (DARR100), given in Fig. 2a, shows contributions from both capsid and DNA resonances, and distinction between them can be clearly observed in the additional Figs. 3 and 4.

Assignment of DNA bases

We assigned all carbons and most of the nitrogens in the DNA bases in a nucleotide-type specific manner using ^{13}C–^{13}C homonuclear DARR100 and ^{15}N–^{13}C heteronuclear TEDOR correlation experiments. A few remaining tertiary amines were assigned from the one-dimensional (1D) ^{15}N CPMAS spectrum (not shown). Since DARR

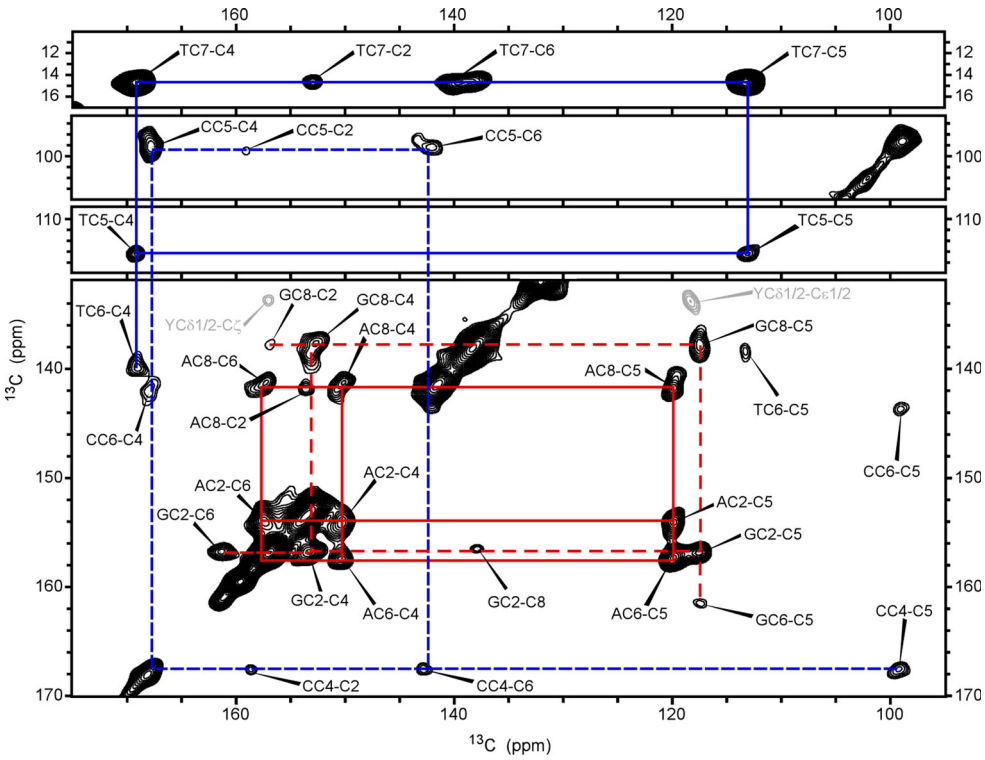

Fig. 3 2D ^{13}C–^{13}C DARR100 spectrum of $^{13}C/^{15}N$ uniformly labeled wild-type T7 phage. The spectrum is shown truncated to the regions of the DNA bases. Indicated on the figure are the assignment patterns of the dT/dC bases (*blue*, *solid/dashed lines*), and the dA/dG bases (*red*, *solid/dashed lines*). All the base carbons were assigned in a nucleotide-type specific manner, thus each cross-peak of a specific nucleobase is an average of approximately 20 thousand sites. A Lorentz-to-Gauss transformation was applied in both dimensions. The numbering scheme of the nucleotides is shown in Fig. 4 below. Capsid resonances are *colored* in *grey*

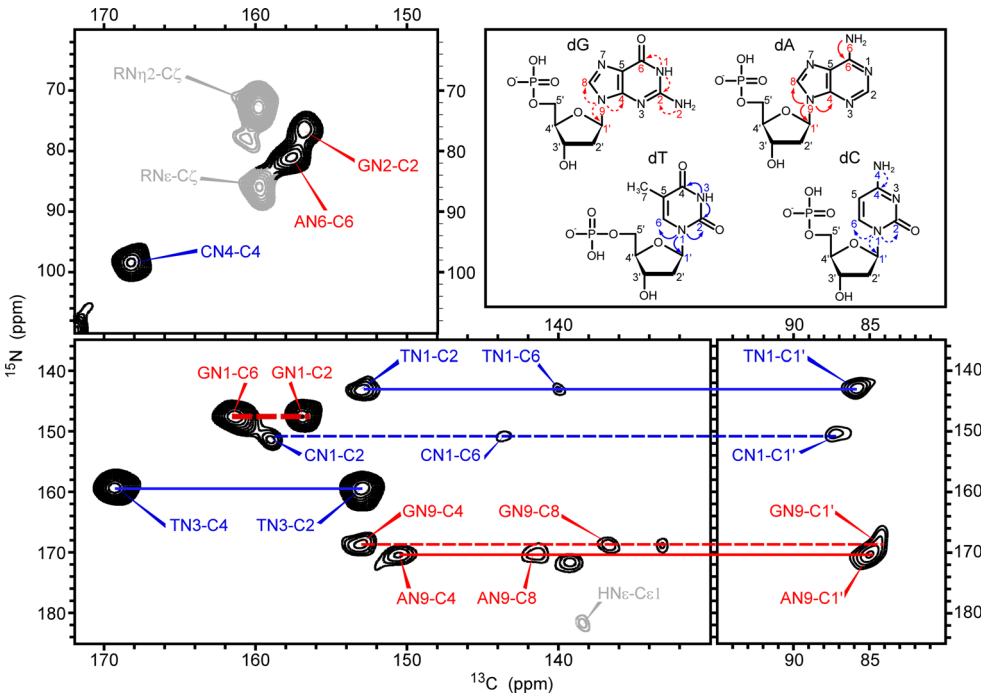

Fig. 4 2D ^{15}N–^{13}C TEDOR spectrum of $^{13}C/^{15}N$ uniformly labeled wild-type T7 phage. The attained correlations are between the protonated and glycosidic nitrogen atoms of the bases and the neighboring carbons. The *top right square* shows the common nomenclature for nucleotides, and *arrows* indicate connections between assigned nitrogens and carbons that are one-bond apart for the dA/dG (*red*) and dT/dC (*blue*) nucleotides. The spectrum was processed with a Lorentz-to-Gauss transformation in both dimensions. The identity of two signals in the vicinity of N9–C8 cross-peaks could not be obtained since no analogue was found in the 2D DARR spectra

depends on proton-assisted magnetization transfer, and many DNA base carbons are quaternary, many cross-peaks between protonated and unprotonated atoms become non-symmetric across the diagonal, some non-protonated nuclei have very weak autocorrelation peaks and in some instances, only a single cross-peak appears in the spectrum. Mostly, cross-peaks result from excitation of protonated carbons or carbons attached to the primary amine groups—C4 of the cytosine base, C2 of guanine and C6 of adenine. These trends are emphasized in Fig. 2b and c, where the DNA region of the DARR100 spectrum, and a graphical summary of the cross-peak identities, are shown. Similarly,

in the TEDOR experiment the most intense correlations were attained between the protonated nitrogens of the bases and neighboring carbons, although the nitrogen atoms connecting the base and sugar moieties were readily observed. The assignment patterns of the DNA bases are shown in Figs. 3 and 4, corresponding to ^{13}C–^{13}C and ^{15}N–^{13}C correlation experiments, respectively.

Thymine bases (dT) were easily assigned through their unique methyl group (dTC7) correlations with all other carbons. Other bases depict a relatively small chemical shift dispersion; however, one distinctive resonance in each base was sufficient to attain the full cross-peak pattern for each type of base. For example, the unique chemical shifts of the aminated C4 and in particular the protonated C5 in cytosine (dC) facilitated its assignment. Adenine (dA) and guanine (dG) bases resonate at similar shifts; however, we specifically assigned them through their different C5 and C8 resonances, and obtained the full pattern for both nucleobases.

All the protonated nitrogen atoms were designated unambiguously to their specific base type in the TEDOR experiment. In addition, the glycosidic nitrogen atoms were assigned through their correlations with three adjacent carbons; two belonging to the base (and confirmed by prior assignment from the DARR correlation spectrum shown in Fig. 3) and a third is the C1′ deoxyribose carbon atom. This assignment also allowed us to obtain nucleotide-type specific assignment of C1′. Tertiary nitrogen atoms (resonating at over 200 ppm) could not be detected in the 2D spectrum, nonetheless they could be resolved and therefore assigned in a 1D ^{15}N CP spectrum (not shown). This particular assignment assumed a B-DNA form, which could be deduced directly from other shifts as discussed below.

Assignment of DNA sugars

The deoxyribose ring resonances depend on the nature of the attached base; pyrimidines (dT and dC) and purines (dA and dG) have somewhat different effects on the sugar carbon shifts. The C1′ resonances of dT and dC are shifted downfield, and the C3′, C4′ and C5′ carbons are shifted upfield, compared with dA and dG. We were able to assign the deoxyribose carbon signals in a nucleotide-type specific manner. The identification was done through specific sugar-base correlations, most of which are shown in Fig. 5 below, or through sugar–sugar cross-peaks. Small differences (in the order of $\sim$1 ppm) between dT and dC, or between dG and dA, were resolved only from sugar-base correlations. C1′ and C4′ of dT/dC, which have similar shifts, could not be resolved in the carbon spectrum. Nevertheless, C1′ shifts of all nucleotides could be assigned to their particular nucleotides in the TEDOR spectrum (Fig. 4) through their attached nitrogens.

Experimental chemical shifts of the T7 dsDNA, deposited in the BMRB under accession code 19805, are given in Table 2, and compared to two data sets; the reported literature shifts of B-DNA, and those of fd (Morag et al. 2014), recently deposited in the BMRB (accession code 19734). Most resonances detected in our spectrum show deviations of up to 0.3 ppm and typical linewidths within 2 ppm, indicative of a highly ordered DNA structure. There are very few exceptions, as shown in the assignment Table 2, which have shifts with a standard deviation of 0.4 ppm or more. For dTC6 and dCC6, a possible minor conformation was observed in some cases; for dTC6, an additional minor conformation appears at a chemical shift, which is 1.5 ppm upfield from the more intense signals given in Table 2. This splitting is visible mainly in the dTC6-C7 cross-peak (Fig. 3) but also in other instances. In the case of dCC6, a correlation with C5 shows an additional signal shifted by +1.2 ppm. In the following, we will discuss the similarities and significance of the differences between the shifts of the nucleotide types in the dsDNA of T7 phage and those of B-DNA and fd phage.

Chemical shifts of the dsDNA in T7 are consistent with a B-form DNA

The conformation of a B-form DNA is characterized by a C2′-endo sugar ring pucker, an *anti* orientation of the glycosidic bond, and by defined dimensions governed by Watson–Crick (WC) base pairing and stacking interactions. Carbon NMR is potentially a great reporter of these characteristics and thus the overall DNA conformation can be determined from ^{13}C, ^{15}N and ^{1}H chemical shift values (see (Lam and Chi 2010) and references within). For RNA, the relationship between ^{13}C sugar chemical shifts and the ribose conformation was further studied by constructing canonical coordinates, which yielded the most probable sugar pucker and glycosidic torsion angle conformation from NMR data (Ebrahimi et al. 2001; Rossi and Harbison 2001). This method was applied for the structural analysis of several RNA systems (Fürtig et al. 2004; Ohlenschläger et al. 2008; Cherepanov et al. 2010); however, such analysis is not straightforward for deoxyribose molecules since the sugar carbons have different average shifts, in particular C2′, which differs by over 30 ppm on average. Thus, in the current study, our experimental chemical shifts are compared to the previous reported values of B-DNA, and to chemical shift trends reported previously for the various nucleotide atoms, most of which were measured by solution NMR studies of short synthesized oligonucleotides.

The deoxyribose ring conformation has a strong correlation with sugar carbons chemical shifts. Previous ^{13}C SSNMR experiments on a series of crystalline nucleotides reported that the C3′-endo conformation is characterized by

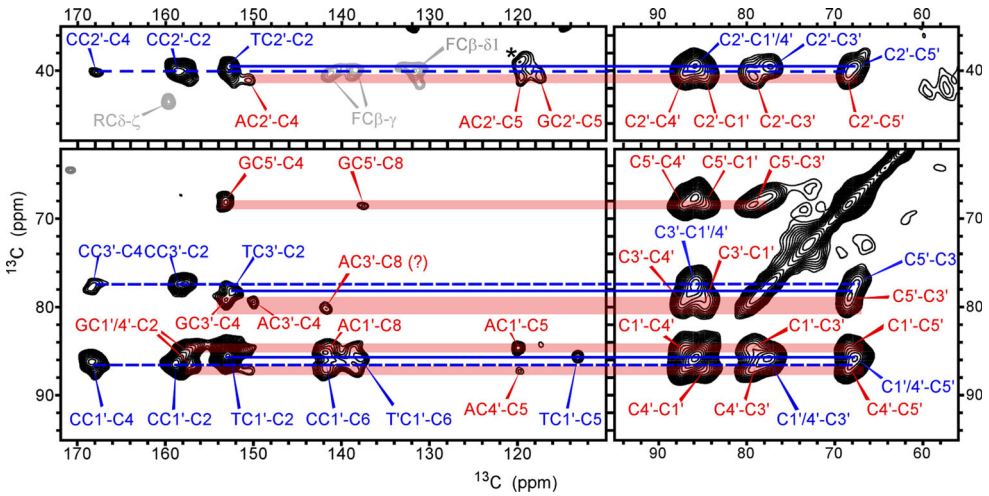

Fig. 5 Extracted regions from DARR100 showing intra-nucleotide correlations of the deoxyribose ring (right, 67–87, 40 ppm), and contacts between sugar and base carbons (*left*). The connections between the dA/dG and dT/dC sugar and base resonances are indicated in *red stripes* and in *blue lines*, respectively. Generally, the variations between the sugar carbons chemical shifts of the different nucleobases are resolved according to the two systems of dA/dG and dT/dC in the sugar region. The slight variations within each system could only be resolved in the sugar-base correlations region, and are more pronounced within the dT/dC system. The *asterisk* denotes a spinning sideband

significant upfield C3′ and C5′ shifts (5–10 ppm) compared to the C3′-exo and C2′-endo conformations (Santos et al. 1989; Xu et al. 1998). The latter two equilibrium conformations can be distinguished to some extent by smaller differences in the C2′ and C4′ shifts. The experimental values of the sugar carbons in T7 dsDNA are consistent with either the C2′-endo or C3′-exo conformations, or a combination of both. The C3′-endo conformation is safely excluded since the average C3′ and C5′ have high chemical shift values.

The glycosidic torsion angle χ, which defines the base orientation (*anti* or *syn* relative to the sugar ring), is also an important factor affecting the ^{13}C and ^{15}N chemical shifts of specific sugar and base atoms (Ghose et al. 1994; Greene et al. 1995; Lam and Chi 2010). It was previously observed (Greene et al. 1995) that for a *syn* orientation the C1′, C3′ and C4′ shift to a lower field (on average 5, 5.6 and 1.5 ppm, respectively), while C2′ resonates at a higher field (7 ppm). In T7, the C1′ shift of dG and dA are clearly consistent with an *anti* conformation, C2′ resonate at ~40–41 ppm, which is similar to average B-DNA values and somewhat lower than the values reported in Greene et al. (1995). Overall, C2′ shifts (and C3′ but this resonance is also affected significantly by the sugar pucker) are also consistent with an *anti* conformation, as expected for a B-form DNA duplex. Base carbons are also affected to some extent by the glycosidic angle, especially dGC8 which is shifted downfield for a *syn* orientation compared to *anti* in a DNA with a C2′-endo sugar pucker (Fonville et al. 2012). The dGC8 resonance was reported to be shifted +2.4 ppm in *syn* compared to *anti*, dGC4 by +0.65 and dGC5 by +1.15 (Greene et al. 1995). Our experimental dGC4, dGC5 and dGC8 are shifted upfield by 2.6, 1.8 and 3.8 ppm, respectively, compared to the average *syn* values reported by Greene et al. (1995). Thus, they are consistent with the *anti* conformation as well. Also consistent with an *anti* conformation are the dGN7 and dGN9 shifts, since usually the *syn* base atoms are shifted upfield (~6 ppm on average for N7 and ~4 ppm for N9) relative to *anti* bases.

A double helix B-form DNA is expected to show typical WC base pairing and in addition to exhibit stacking interactions, which are also responsible for its stabilization. These interactions affect the observed carbon and nitrogen shifts (Hu et al. 1998; Farès et al. 2007; Malináková et al. 2010). It was reported that the dGC2, dGC6 and dTC4 are deshielded (~1 ppm) upon WC pairing in oligodeoxynucleotide duplexes (Borer et al. 1988; LaPlante et al. 1988). Although these shifts are small, our results are consistent with the values that were reported for base paired oligonucleotides. It should be pointed out that base stacking tends to shield base carbons, while hydrogen bond formation usually causes a deshielding effect. However, the combination of these two opposite trends yields a net deshielding effect on carbons that are near the hydrogen bonding sites.

Limited ^{15}N NMR assignments of the participating nitrogens in WC hydrogen bonding in DNA were published, mainly of small DNA molecules including short duplexes and hairpins (Fernández et al. 1998; Pervushin et al. 1998; Padrta et al. 2002). It is found that the imino guanine nitrogen (dGN1) atoms, involved in WC pairing as H donors, resonate at an average value of 147.4 ppm,

Table 2 ^{13}C and ^{15}N assignment list of the dsDNA in wild-type T7 bacteriophage

Atom	Exp. dsDNA in T7	B-form oligomers	ssDNA in fd
TC1′	85.6	84.5 (1.1)	85.7
TC2′	39.3	39.3 (0.6)	39.3
TC3′	77.8	76.7 (1.8)	80.1
TC4′	Overlap C1′	85.0 (1.5)	86.8
TC5′	67.6	66.3 (1.6)	68.0
TC2	152.9	151.6	153.4
TC4	169.1	166.8	168.5
TC5	113.2	112.1	113.6
TC6	139.8[a]	138.2 (1.4)	139.2
TC7	14.6	13.7 (1.3)	14.4
TN1	142.9	–	–
TN3	159.2	159.1[b]	–
CC1′	86.9 (0.4)	85.6 (1.4)	84.6–88.6
CC2′	40.1	40.5 (0.9)	40.3
CC3′	77.2	74.8 (3.1)	80.3
CC4′	Overlap C1′	86.7 (1.5)	84.6–88.4
CC5′	67.6[c]	66.8 (1.6)	68.1
CC2	158.8	159.5	159.2
CC4	167.8	168.5	168.0
CC5	99.1	98.4 (0.8)	99.2
CC6	142.2 (0.5)	142.9 (0.8)	142.2
CN1	150.7 (0.4)	–	–
CN3	196.3	–	–
CN4	98.2	97.1[b]	–
GC1′	84.5	83.5 (1.4)	85.6
GC2′	40.6	41.3 (0.9)	38.9
GC3′	79.2	77.6 (2.5)	80.6
GC4′	86.6	86.4 (2.3)	87.4
GC5′	68.3	67.1(1.9)	68.1
GC2	156.7	156.4	156.5
GC4	153.1	153.6	154.0
GC5	117.4	118.6	117.6
GC6	161.4	161.2	161.0
GC8	137.5 (0.4)	138.0 (1.2)	138.6
GN1	147.4	147.4[b]	–
GN2	76.1	75.1[b]	–
GN7	238.3	236.9[b]	–
GN9	168.5	–	–
AC1′	84.9	83.7 (1.2)	85.6
AC2′	40.8	40.5 (0.3)	40.0
AC3′	79.4	78.4 (1.5)	80.0
AC4′	86.8	86.6 (1.4)	87.4
AC5′	68.4	68.2	68.2
AC2	154.0	153.7 (1.3)	154.6
AC4	150.3	149.7	150.6
AC5	119.9	118.6	119.8
AC6	157.4	156.7	157.0
AC8	141.6	140.7 (1.3)	141.2
AN1	223.4	225.2[b]	–
AN3	214.5	216.4[b]	–
AN6	80.8	80.2[b]	–
AN7	234.1	233.5[b]	–
AN9	170.2	–	–

The experimental values (exp.) are given in ppm, and are compared to two data references; the average shifts of B-form oligomers from several sources (Sergeyev et al. 2011), and the recently reported assignment of the ssDNA in the filamentous fd phage. Most experimental values are held within 0.3 ppm, apart from few exceptions, indicated in the table with their standard deviations. The standard deviations of B-DNA oligomers are indicated in parenthesis for assignments with over 5 entries

[a] The signal of TC6 appears to have an additional minor conformation in 138.3. This resonance can be observed in Fig. 3 (a correlation to TC7), and in a TEDOR spectrum that is apodized with a large broadening factor (not shown)

[b] Average nitrogen shifts from BMRB entries of B-form oligonucleotides

[c] CC5′ overlaps with TC5′; however TC5′ can be separately resolved (via TC4 in an exponentially apodized spectrum)

consistent with the value observed in T7. Our assignments of imino dTN3, and amino dAN6, dCN4 and dGN2 also lay within a deviation of ~1 ppm compared to the shifts of model duplex DNA systems. Generally, the imino and amino nitrogen resonances of nucleotides involved in WC base pairs are found at a lower field than those originating from non-base paired nucleotides (Dieckmann and Feigon 1997). For example, in a study of G-tetrad DNA, the hydrogen bonding between dGN1 and dGO6 (known as Hoogsteen H-bonding) was observed, and the resonances of N1 in four dG bases were at 143–145 ppm (Liu et al. 2000), upfield compared to the shifts obtained in nucleotides with WC pairing. The unprotonated nitrogens, which act as H-bond acceptors are also important; however, chemical shift information on these is lacking. Generally, it is suggested that they are shifted towards higher fields upon H-bond formation (~10 ppm), while an average value is around 230 ppm (without H-bonding). For example, dAN1 in T7 resonate at chemical shifts that are upfielded ~13 ppm, respectively, compared to the reported assigned shifts in adenosine nucleotides, where hydrogen bonds are absent (Cho and Evans 1991). Similar trends were also observed in a 14-mer DNA duplex where H-bonded dAN1 and dCN3 acceptors are obtained at upfield values of ~222 and ~196 ppm (Pervushin et al. 1998). Studies on RNA molecules, which contain different H-bonds, also help in the interpretation of chemical shifts. For example, a study

on $(CUG)_{97}$ RNA reported, through MAS SSNMR experiments, a correlation peak between dGN1 and dCN3 (at ~147 and ~196 ppm) suggesting the presence of a canonical GC Watson–Crick base pairing (Leppert et al. 2004). Our dGN1 resonance (147.4 ppm) is in agreement with the reported assignments thus indicating the presence of WC base pairing.

Overall, the chemical shift values for the encapsulated T7 dsDNA report on a C2′-endo (or C3′-exo) sugar conformation, an *anti* orientation for the glycosidic bond, and indicate the presence of WC base pairing. All of these are the expected structural characteristic of a B-form DNA, as was reported from Raman studies. Nevertheless, the database from which this information is obtained is limited, quaternary carbon shifts are scarce and therefore this study presents an additional source for comparison and as a basis to study other large native DNA systems.

Comparison to fd, a ssDNA filamentous bacteriophage

Recently, we reported on the ^{13}C chemical shifts of the circular ssDNA encapsulated in fd virus using MAS SSNMR (Morag et al. 2014). In the study of its genome, which contains slightly over 6,000 bases and therefore is much smaller than T7, it was found to have an S-type sugar pucker (C2′-endo or C3′-exo) and a probable *anti* base orientation. The reported shifts also indicated the presence of hydrogen bonding between the bases. Despite the differences in size, packing and probably the nature of H-bonding, the two phages (fd and T7) share surprisingly similar secondary structure features, as seen from the similarities of their ^{13}C resonances (see Table 2). The main differences are observed for the sugar C3′, C4′ and C5′ carbons, which take consistently higher values for fd (except dAC5′), and for both T7 and fd the shifts are in the high end of B-form shifts, yet within their standard deviation. The base (carbon) shifts for both systems are very similar and differences in the order of ~1 ppm have been observed only for dGC4 and dGC8. These trends cannot be easily explained so far and it is remained to be examined on other systems, and by calculations, whether they are related to the size of the genome, to the strained DNA forms, or to any other genome packaging properties.

Conclusion

The small number of nucleotides, small chemical shift variability, and the lack of a dense proton network in nucleotides, pose limitations on NMR data acquisition and interpretation of polynucleic acids, both in solid and solution states. While most DNA and RNA studies were reported from solution NMR, analysis is restricted to low-molecular-weight molecules. In the solid state, where molecular weight does not limit spectral resolution, site-specific assignment of over tens of thousands of nucleotides is impractical. Moreover, signal intensities of protonless heteroatoms (i.e. carbons and nitrogens) are low compared to the protonated atoms. The outcome of these limitations is a poor chemical shift NMR knowledge of large and natural genomes.

In this contribution, we showed that nucleotide-type specific assignment of a large DNA system, the 40 kbp dsDNA in T7 phage, can be readily obtained by solid-state MAS NMR. The complete ^{13}C and near complete ^{15}N assignment was based on two 2D data sets. Despite multiple repeats of the deoxyribose nucleotides (about twenty thousand bases for each of the dA, dG, dT, dC building blocks), and their high compaction, spectral cross-peaks were surprisingly narrow and well resolved, indicating a highly ordered packaged DNA. Normally, a calculation of the secondary structure can be done with high fidelity if there is a reliable chemical shift database. However, for dsDNA systems, in particular of large systems, such studies are scarce. Our study of the dsDNA in T7 phage serves therefore as a starting point in constructing a reliable chemical shift database for large native DNA molecules, and adds to the group of recently reported studies of the ssDNA in fd (Morag et al. 2014) and Pf1 (Sergeyev et al. 2011) filamentous phages. We have already observed here some common effects on the NMR properties of large DNA systems and we anticipate that these results will accelerate efforts towards the characterization of more complex DNA and RNA in the context of real biological entities by MAS NMR.

Acknowledgments We would like to thank Dr. Udi Qimron from the Department of Human Microbiology, Faculty of Medicine in Tel Aviv University, for providing initial stocks of wild-type T7 phage and its host. We thank Anat Haimovich for the TEDOR simulations. Financial support was provided by the Israel Science Foundation. Partial support for the spectrometer was given by the center for Nanoscience and Nanotechnology of Tel Aviv University.

References

Abramov G, Morag O, Goldbourt A (2011) Magic-angle spinning NMR of a class I filamentous bacteriophage virus. J Phys Chem B 115:9671–9680

Aeschbacher T, Schmidt E, Blatter M et al (2013) Automated and assisted RNA resonance assignment using NMR chemical shift statistics. Nucleic Acids Res 41:e172

Agirrezabala X, Martín-Benito J, Castón JR et al (2005) Maturation of phage T7 involves structural modification of both shell and inner core components. EMBO J 24:3820–3829

Aitken A, Learmonth M (1996) Protein determination by UV absorption. In: Walker JM (ed) Protein Protoc. Handb. Humana Press, Totowa, pp 3–6

Asami S, Rakwalska-Bange M, Carlomagno T, Reif B (2013) Protein-RNA interfaces probed by ^{1}H-detected MAS solid-state NMR spectroscopy. Angew Chem Int Ed Engl 52:2345–2349

Barton S, Heng X, Johnson BA, Summers MF (2013) Database proton NMR chemical shifts for RNA signal assignment and validation. J Biomol NMR 55:33–46

Ben-Shaul A (2013) Entropy, energy, and bending of DNA in viral capsids. Biophys J 104:L15–L17

Berjanskii MV, Neal S, Wishart DS (2006) PREDITOR: a web server for predicting protein torsion angle restraints. Nucleic Acids Res 34:W63–W69

Black LW, Thomas JA (2012) Condensed genome structure. Adv Exp Med Biol 726:469–487

Borer PN, LaPlante SR, Zanatta N, Levy GC (1988) Hydrogen-bonding effects and ^{13}C-NMR of the DNA double helix. Nucleic Acids Res 16:2323–2332

Cady SD, Schmidt-Rohr K, Wang J et al (2010) Structure of the amantadine binding site of influenza M2 proton channels in lipid bilayers. Nature 463:689–692

Cerritelli M, Cheng N, Rosenberg A et al (1997) Encapsidated conformation of bacteriophage T7 DNA. Cell 91:271–280

Cerritelli ME, Trus BL, Smith CS et al (2003) A second symmetry mismatch at the portal vertex of bacteriophage T7: 8-fold symmetry in the procapsid core. J Mol Biol 327:1–6

Cherepanov AV, Glaubitz C, Schwalbe H (2010) High-resolution studies of uniformly ^{13}C,^{15}N-labeled RNA by solid-state NMR spectroscopy. Angew Chem Int Ed Engl 49:4747–4750

Cho BP, Evans FE (1991) Structure of oxidatively damaged nucleic acid adducts. 3. Tautomerism, ionization and protonation of 8-hydroxyadenosine studied by ^{15}N NMR spectroscopy. Nucleic Acids Res 19:1041–1047

Cornilescu G, Delaglio F, Bax A (1999) Protein backbone angle restraints from searching a database for chemical shift and sequence homology. J Biomol NMR 13:289–302

Cuervo A, Pulido-Cid M, Chagoyen M et al (2013) Structural characterization of the bacteriophage T7 tail machinery. J Biol Chem 288:26290–26299

Daudén MI, Martín-Benito J, Sánchez-Ferrero JC et al (2013) Large terminase conformational change induced by connector binding in bacteriophage T7. J Biol Chem 288:16998–17007

Day LA, Marzec CJ, Reisberg SA, Casadevall A (1988) DNA packing in filamentous bacteriophages. Annu Rev Biophys Biophys Chem 17:509–539

Dayie KT (2005) Resolution enhanced homonuclear carbon decoupled triple resonance experiments for unambiguous RNA structural characterization. J Biomol NMR 32:129–139

De Groot HJ (2000) Solid-state NMR spectroscopy applied to membrane proteins. Curr Opin Struct Biol 10:593–600

Delaglio F, Grzesiek S, Vuister GW et al (1995) NMRPipe: a multidimensional spectral processing system based on UNIX pipes. J Biomol NMR 6:277–293

Deng H, Bloomfield V, Benevides J, Thomas G (1999) Dependence of the Raman signature of genomic B-DNA on nucleotide base sequence. Biopolymers 50:656–666

Dieckmann T, Feigon J (1997) Assignment methodology for larger RNA oligonucleotides: application to an ATP-binding RNA aptamer. J Biomol NMR 9:259–272

Duda RL, Ross PD, Cheng N et al (2009) Structure and energetics of encapsidated DNA in bacteriophage HK97 studied by scanning calorimetry and cryo-electron microscopy. J Mol Biol 391:471–483

Ebrahimi M, Rossi P, Rogers C, Harbison GS (2001) Dependence of ^{13}C NMR chemical shifts on conformations of RNA nucleosides and nucleotides. J Magn Reson 150:1–9

Farès C, Amata I, Carlomagno T (2007) ^{13}C-detection in RNA bases: revealing structure-chemical shift relationships. J Am Chem Soc 129:15814–15823

Fernández C, Szyperski T, Ono A et al (1998) NMR with ^{13}C, ^{15}N-doubly-labeled DNA: the Antennapedia homeodomain complex with a 14-mer DNA duplex. J Biomol NMR 12:25–37

Fiala R, Munzarová M, Sklenář V (2004) Experiments for correlating quaternary carbons in RNA bases. J Biomol NMR 29:477–490

Fonville JM, Swart M, Vokáčová Z et al (2012) Chemical shifts in nucleic acids studied by density functional theory calculations and comparison with experiment. Chem Eur J 18:12372–12387

Fürtig B, Richter C, Wöhnert J, Schwalbe H (2003) NMR spectroscopy of RNA. ChemBioChem 4:936–962

Fürtig B, Richter C, Bermel W, Schwalbe H (2004) New NMR experiments for RNA nucleobase resonance assignment and chemical shift analysis of an RNA UUCG tetraloop. J Biomol NMR 28:69–79

Ghose R, Marino JP, Wiberg KB, Prestegard JH (1994) Dependence of ^{13}C chemical shifts on glycosidic torsional angles in ribonucleic acids. J Am Chem Soc 116:8827–8828

Goddard TD, Kneller DG (2008) SPARKY 3. University of California, San Francisco

Goldbourt A, Gross BJ, Day LA, McDermott AE (2007) Filamentous phage studied by magic-angle spinning NMR: resonance assignment and secondary structure of the coat protein in Pf1. J Am Chem Soc 129:2338–2344

Goldfarb A, Saidel L, Mosovich E (1951) The ultraviolet absorption spectra of proteins. J Biol Chem 193:397–404

Greene KL, Wang Y, Live D (1995) Influence of the glycosidic torsion angle on ^{13}C and ^{15}N shifts in guanosine nucleotides: investigations of G-tetrad models with alternating syn and anti bases. J Biomol NMR 5:333–338

Han Y, Hou G, Suiter CL et al (2013) Magic angle spinning NMR reveals sequence-dependent structural plasticity, dynamics, and the spacer peptide 1 conformation in HIV-1 capsid protein assemblies. J Am Chem Soc 135:17793–17803

Henderson JT, Benight AS, Hanlon S (1992) A semi-micromethod for the determination of the extinction coefficients of duplex and single-stranded DNA. Anal Biochem 201:17–29

Hing AW, Vega S, Schaefer J (1992) Transferred-echo double-resonance NMR. J Magn Reson 96:205–209

Hu JZ, Facelli JC, Alderman DW et al (1998) ^{15}N Chemical shift tensors in nucleic acid bases. J Am Chem Soc 120:9863–9869

Ionel A, Velázquez-Muriel JA, Luque D et al (2011) Molecular rearrangements involved in the capsid shell maturation of bacteriophage T7. J Biol Chem 286:234–242

Jaroniec CP, MacPhee CE, Bajaj VS et al (2004) High-resolution molecular structure of a peptide in an amyloid fibril determined by magic angle spinning NMR spectroscopy. Proc Natl Acad Sci U S A 101:711–716

Jehle S, Falb M, Kirkpatrick JP et al (2010) Intermolecular protein-RNA interactions revealed by 2D ^{31}P–^{15}N magic angle spinning solid-state NMR spectroscopy. J Am Chem Soc 132:3842–3846

Jiang W, Chang J, Jakana J et al (2006) Structure of epsilon15 bacteriophage reveals genome organization and DNA packaging/injection apparatus. Nature 439:612–616

Lam SL, Chi LM (2010) Use of chemical shifts for structural studies of nucleic acids. Prog Nucl Magn Reson Spectrosc 56:289–310

LaPlante SR, Boudreau EA, Zanatta N et al (1988) ^{13}C NMR of the bases of three DNA oligonucleotide duplexes: assignment methods and structural features. Biochemistry 27:7902–7909

Leppert J, Urbinati CR, Häfner S et al (2004) Identification of NH…N hydrogen bonds by magic angle spinning solid state NMR in a double-stranded RNA associated with myotonic dystrophy. Nucleic Acids Res 32:1177–1183

Liu A, Majumdar A, Hu W et al (2000) NMR detection of NH···OC hydrogen bonds in ^{13}C, ^{15}N-labeled nucleic acids. J Am Chem Soc 122:3206–3210

Lopez del Amo JM, Schmidt M, Fink U et al (2012) An asymmetric dimer as the basic subunit in Alzheimer's disease amyloid β fibrils. Angew Chem Int Ed Engl 51:6136–6139

Loquet A, Sgourakis NG, Gupta R et al (2012) Atomic model of the type III secretion system needle. Nature 486:276–279

Malináková K, Novosadová L, Lahtinen M et al (2010) ^{13}C chemical shift tensors in hypoxanthine and 6-mercaptopurine: effects of substitution, tautomerism, and intermolecular interactions. J Phys Chem A 114:1985–1995

Marchanka A, Simon B, Carlomagno T (2013) A suite of solid-state NMR experiments for RNA intranucleotide resonance assignment in a 21 kDa protein-RNA complex. Angew Chemie 125:10180–10185

McDermott A, Gu Z (1996) Carbon and nitrogen chemical shifts: applications to solid state proteins. Encycl Nucl Magn Reson 1137–1147

Morag O, Abramov G, Goldbourt A (2014) Complete chemical shift assignment of the ssDNA in the filamentous bacteriophage fd reports on its conformation and on its interface with the capsid shell. J Am Chem Soc 136:2292–2301

Morcombe CR, Zilm KW (2003) Chemical shift referencing in MAS solid state NMR. J Magn Reson 162:479–486

Morcombe CR, Gaponenko V, Byrd RA, Zilm KW (2004) Diluting abundant spins by isotope edited radio frequency field assisted diffusion. J Am Chem Soc 126:7196–7197

Ohlenschläger O, Haumann S, Ramachandran R, Görlach M (2008) Conformational signatures of ^{13}C chemical shifts in RNA ribose. J Biomol NMR 42:139–142

Overman SA, Aubrey KL, Reilly KE et al (1998) Conformation and interactions of the packaged double-stranded DNA genome of bacteriophage T7. Biospectroscopy 4:S47–S56

Padrta P, Stefl R, Králík L et al (2002) Refinement of d(GCGAAGC) hairpin structure using one- and two-bond residual dipolar couplings. J Biomol NMR 24:1–14

Park SH, Das BB, Casagrande F et al (2012) Structure of the chemokine receptor CXCR1 in phospholipid bilayers. Nature 491:779–783

Pervushin K, Ono A, Fernández C et al (1998) NMR scalar couplings across Watson-Crick base pair hydrogen bonds in DNA observed by transverse relaxation-optimized spectroscopy. Proc Natl Acad Sci U S A 95:14147–14151

Petkova AT, Ishii Y, Balbach JJ et al (2002) A structural model for Alzheimer's beta-amyloid fibrils based on experimental constraints from solid state NMR. Proc Natl Acad Sci U S A 99:16742–16747

Petkova AT, Yau W-M, Tycko R (2006) Experimental constraints on quaternary structure in Alzheimer's beta-amyloid fibrils. Biochemistry 45:498–512

Petrov AS, Boz MB, Harvey SC (2007) The conformation of double-stranded DNA inside bacteriophages depends on capsid size and shape. J Struct Biol 160:241–248

Pines A, Gibby M, Waugh J (1973) Proton-enhanced NMR of dilute spins in solids. J Chem Phys 59:569–590

Porterfield JZ, Zlotnick A (2010) A simple and general method for determining the protein and nucleic acid content of viruses by UV absorbance. Virology 407:281–288

Richter C, Kovacs H, Buck J et al (2010) ^{13}C-direct detected NMR experiments for the sequential J-based resonance assignment of RNA oligonucleotides. J Biomol NMR 47:259–269

Riedel K, Leppert J, Häfner S et al (2004) Homonuclear chemical shift correlation in rotating solids via RN^{ν}_{N} symmetry-based adiabatic RF pulse schemes. J Biomol NMR 30:389–395

Riedel K, Leppert J, Ohlenschläger O et al (2005) TEDOR with adiabatic inversion pulses: resonance assignments of ^{13}C/^{15}N labelled RNAs. J Biomol NMR 31:49–57

Rossi P, Harbison GS (2001) Calculation of ^{13}C chemical shifts in RNA nucleosides: structure-^{13}C chemical shift relationships. J Magn Reson 151:1–8

Sambrook J, Fritsch EF, Maniatis T (1989) Molecular cloning: a laboratory manual, 2nd edn. Cold Spring Harbor Laboratory Press, Cold Spring Harbor

Santos RA, Tang P, Harbison GS (1989) Determination of the DNA sugar pucker using ^{13}C NMR spectroscopy. Biochemistry 28:9372–9378

Schmid F (2001) Biological Macromolecules: UV-visible Spectrophotometry. Encycl Life Sci 1–4

Sergeyev IV, Day LA, Goldbourt A, McDermott AE (2011) Chemical shifts for the unusual DNA structure in Pf1 bacteriophage from dynamic-nuclear-polarization-enhanced solid-state NMR spectroscopy. J Am Chem Soc 133:20208–20217

Shen Y, Vernon R, Baker D, Bax A (2009) De novo protein structure generation from incomplete chemical shift assignments. J Biomol NMR 43:63–78

Stejskal EO, Schaefer J, Waugh J (1977) Magic-angle spinning and polarization transfer in proton-enhanced NMR. J Magn Reson 28:105–112

Studier FW (1969) The genetics and physiology of bacteriophage T7. Virology 39:562–574

Takegoshi K, Nakamura S, Terao T (2001) ^{13}C–^{1}H dipolar-assisted rotational resonance in magic-angle spinning NMR. Chem Phys Lett 344:631–637

Tang M, Comellas G, Rienstra CM (2013) Advanced solid-state NMR approaches for structure determination of membrane proteins and amyloid fibrils. Acc Chem Res 46:2080–2088

Tataurov AV, You Y, Owczarzy R (2008) Predicting ultraviolet spectrum of single stranded and double stranded deoxyribonucleic acids. Biophys Chem 133:66–70

Thakur RS, Kurur ND, Madhu PK (2006) Swept-frequency two-pulse phase modulation for heteronuclear dipolar decoupling in solid-state NMR. Chem Phys Lett 426:459–463

Thomas GJ, Serwer P (1990) Secondary structure of the double-stranded DNA genome of bacteriophage T7 in packaged, underpackaged and unpackaged states. J Raman Spectrosc 21:569–575

Tomar S, Green MM, Day LA (2007) DNA-protein interactions as the source of large-length-scale chirality evident in the liquid crystal behavior of filamentous bacteriophages. J Am Chem Soc 129:3367–3375

Tóth K, Bolard J, Rontó G, Aslanian D (1984) UV-induced small structural changes in the T7 bacteriophage studied by melting methods. Biophys Struct Mech 10:229–239

Ulrich EL, Akutsu H, Doreleijers JF et al (2008) BioMagResBank. Nucleic Acids Res 36:D402–D408

Veshtort M, Griffin RG (2006) SPINEVOLUTION: a powerful tool for the simulation of solid and liquid state NMR experiments. J Magn Reson 178:248–282

Wang S, Munro RA, Shi L et al (2013) Solid-state NMR spectroscopy structure determination of a lipid-embedded heptahelical membrane protein. Nat Methods 10:1007–1012

Wasmer C, Lange A, Van Melckebeke H et al (2008) Amyloid fibrils of the HET-s(218-289) prion form a beta solenoid with a triangular hydrophobic core. Science 319:1523–1526

Wijmenga SS, van Buuren BNM (1998) The use of NMR methods for conformational studies of nucleic acids. Prog Nucl Magn Reson Spectrosc 32:287–387

Wishart DS, Sykes BD (1994) The ^{13}C chemical-shift index: a simple method for the identification of protein secondary structure using ^{13}C chemical-shift data. J Biomol NMR 4:171–180

Xu X-P, Chiu W-LAK, Au-Yeung SCF (1998) Chemical shift and structure relationship in nucleic acids: correlation of backbone torsion angles γ and α with ^{13}C chemical shifts. J Am Chem Soc 120:4230–4231

Yu T-Y, Schaefer J (2008) REDOR NMR characterization of DNA packaging in bacteriophage T4. J Mol Biol 382:1031–1042